

WANG, S., GAO, H., TAKYI-ANINAKWA, P., GUERRERO, J.M., FERNANDEZ, C. and HUANG, Q. 2024. Improved multiple feature-electrochemical thermal coupling modeling of lithium-ion batteries at low-temperature with real-time coefficient correction. *Protection and control of modern power systems* [online], 9(3), pages 157-173. Available from: <https://doi.org/10.23919/PCMP.2023.000257>

Improved multiple feature-electrochemical thermal coupling modeling of lithium-ion batteries at low-temperature with real-time coefficient correction.

WANG, S., GAO, H., TAKYI-ANINAKWA, P., GUERRERO, J.M., FERNANDEZ, C. and HUANG, Q.

2024

© 2024 IEEE. Personal use of this material is permitted. Permission from IEEE must be obtained for all other uses, in any current or future media, including reprinting/republishing this material for advertising or promotional purposes, creating new collective works, for resale or redistribution to servers or lists, or reuse of any copyrighted component of this work in other works.

Improved Multiple Feature-electrochemical Thermal Coupling Modeling of Lithium-ion Batteries at Low-temperature with Real-time Coefficient Correction

Shunli Wang, *Fellow, IET*, Haiying Gao, Paul Takyi-Aninakwa, Josep M. Guerrero, Carlos Fernandez, and Qi Huang, *Fellow, IEEE*

Abstract—Monitoring various internal parameters plays a core role in ensuring the safety of lithium-ion batteries in power supply applications. It also influences the sustainability effect and online state of charge prediction. An improved multiple feature-electrochemical thermal coupling modeling method is proposed considering low-temperature performance degradation for the complete characteristic expression of multi-dimensional information. This is to obtain the parameter influence mechanism with a multi-variable coupling relationship. An optimized decoupled deviation strategy is constructed for accurate state of charge prediction with real-time correction of time-varying current and temperature effects. The innovative decoupling method is combined with the functional relationships of state of charge and open-circuit voltage to capture energy management effectively. Then, an adaptive equivalent-prediction model is constructed using the state-space equation and iterative feedback correction, making the proposed model adaptive to fractional calculation. The maximum state of charge estimation errors of the proposed method are 4.57% and 0.223% under the Beijing bus dynamic stress test and dynamic stress test conditions, respectively. The improved multiple feature-electrochemical thermal coupling modeling realizes the effective correction of the current and temperature variations with noise influencing coefficient, and provides an efficient state of charge prediction method adaptive to complex conditions.

Index Terms—Adaptive inner state characterization, lithium-ion batteries, low-temperature automatic-guided-vehicle, multiple feature-electrochemical thermal coupling modeling, real-time coefficient correction.

Received: October 16, 2023

Accepted: January 19, 2024

Published Online: May 1, 2024

Shunli Wang (corresponding author) is with the School of Electric Power, Inner Mongolia University of Technology, Inner Mongolia 010051, China; with the School of Information Engineering, Southwest University of Science and Technology, Mianyang 621010, China (e-mail: wangshunli@swust.edu.cn).

DOI: 10.23919/PCMP.2023.000257

I. INTRODUCTION

Lithium-ion batteries are the preferred energy storage system because of their high-power density and recyclability advantages [1]. Rational application can contribute to battery life extension, thereby saving resources and reducing the costs of unnecessary losses [2]–[4]. In addition, service life is closely related to the battery status and the relationship needs to be obtained for a reliable power supply. The state of charge (SOC) value reflects the remaining capacity status of batteries, and when the SOC value is estimated accurately, the battery system is managed with a known remaining capacity, providing an effective way to achieve the optimal performance of the batteries [5]–[7]. Therefore, accurate real-time SOC prediction can provide significant assistance in battery management.

SOC not only provides reference for battery endurance, but also plays a key role in the battery management system (BMS). The accurate prediction of SOC can be used for the calculation and correction of state of health (SOH), state of energy (SOE) and state of power (SOP). However, SOC cannot be observed directly and needs to be estimated through observable variables such as voltage, current, and temperature [8]–[10]. Thus, how to establish the nonlinear mapping relationship between observable variables and SOC is a key problem that must be solved. The traditional methods for estimating SOC include open-circuit voltage (OCV), Ampere-hour (AH) integration, and electrochemical impedance spectroscopy (EIS) [11]. The open-circuit voltage method requires the battery to remain stationary for a long time to obtain the OCV-SOC curve, which is not suitable for online measurement [12], [13]. The Ampere-hour integration method achieves SOC prediction through current integration, but requires high accuracy in sampling [14]–[16]. Electrochemical impedance spectroscopy uses battery impedance for SOC prediction. This requires the battery to be in a stationary

state during the measurement process, making it difficult to implement on site [17]. With the development of new technologies, at present, the commonly used SOC estimation methods include model-based methods and data-driven methods [18]–[21]. Among them, data-driven methods require a large number of test samples and time costs, and therefore, the SOC estimation method based on the combination of model and filter observer has become a research hotspot.

Highly accurate SOC estimation relies on an accurate battery model and expression of internal parameters. The battery has a complicated internal structure with various internal factors such as temperature, resistance, and electrochemical concentration [22], [23]. Therefore, establishing high-precision battery models and adaptive internal parameter identification strategies are the key to accurately estimating the internal state of batteries [24], [25]. As battery modelling research continues to progress, researchers have conducted multi-dimensional research and exploration based on the resistance-capacitance (RC) model of batteries, which to a certain extent enables the characterization and dynamic description of the internal polarization effects of the batteries, as shown in Table I.

TABLE I
THE CONTENTS OF BATTERY MODELS THAT HAVE BEEN STUDIED
BY RESEARCHERS

Researcher	Research contents
Mesbahi et al. [26].	A dynamic model of Li-ion batteries incorporating electrothermal and ageing aspects is proposed for electric vehicle applications.
Barai et al. [27].	It is proposed that the accuracy of the estimation of the internal resistance of a battery is closely related to the time scale of the measurement technique used.
Fridholm et al. [28].	An RLS method to estimate the ohmic internal resistance and an adaptive Kalman filter to estimate the time constants of the dynamic effects is proposed.
Feng et al. [29].	A 3D electrochemical-thermal model which predict the voltage and temperature responses of the battery with or without internal short circuit (ISC) is built to simulate various ISC scenarios inside a large format lithium ion battery.
Bruch et al. [30].	A novel approach to extract the equivalent circuit model parameter from a pulse test is proposed.
Fenner et al. [31].	A battery voltage model called 4-KiVM is proposed for variable operating conditions.
Ruan et al. [9].	A novel electrochemical model-based quantitative analysis method of performance decrease and fast-charging limitation for LIBs at low temperatures is proposed.

High-precision battery state evaluation depends on the high-precision model and internal parameters. Battery modeling under low-temperature conditions is challenging and the following key steps need to be taken: first, a description of the interaction and coupling relationship between model parameters should be conducted. The model parameters of ohmic and polariza-

tion resistance, and polarization capacitance need to be measured indirectly by experiment, as their mathematical descriptions can only be realized by external parameters such as voltage, current, and temperature [32], [33]. However, most existing studies do not consider the influence of the coupling relationship between the parameters on the modeling accuracy. Secondly, the influence correction of the low-temperature environmental disturbance should be performed on the model [34], [35]. Because of the low-temperature influence, the external measurement parameters contain multiple uncertain noise information [36], [37]. Thus, how to suppress the noise interference in complex scenes and how to quickly build a reliable mathematical equation need to be established urgently. Thirdly, note that the inconsistency of multi-time-scale model parameter identification results between polarization impedances is significant [38]–[42].

The time-domain equivalent circuit modeling method has high accuracy by identifying model parameters through limited dynamic conditions, and the time-domain parameter matching techniques may have the adaptability problem of varying conditions. Short-time scale state parameter estimation, such as SOC, SOE, and SOP, plays an important supporting role in improving the evaluation results of battery performance and long-timescale RUL prediction accuracy [43]–[45]. Compared with easily measured parameters such as voltage, current, and temperature, these state parameters that can effectively characterize the battery characteristics are difficult to estimate accurately [46]. Therefore a large number of state parameter estimation models have been constructed [47]–[49], including the extended Kalman filter (EKF), particle filter (PF), and neural network (NN). Among them, the Kalman filter and its improved algorithms, including the unscented Kalman (UKF), adaptive Kalman (AKF), and dual Kalman filters (DKF), are widely used in battery state estimation because of their strong robustness and anti-interference ability.

The EKF-based method is introduced for its strong adaptability characteristics. It is constructed with the variational Bayesian approximation for SOC prediction with the modeling parameters [50], [51]. The sampling frequency influences the optimization effect, and a modeling accuracy is proposed to validate the capacity prediction accuracy for an in-loop testing method [52], whereas the incremental capacity is analyzed with a differential voltage description of the SOC and capacity co-prediction [53]. The calculation formulas are formed for the current collection method with the aging condition and current rates, which have cumulative effects on the long-term integration and prediction results. Thus, the prediction error continues to expand over a long sampling time, causing the estimated value to deviate from the actual value variation, resulting in an error degree that increases monotonically [54], [55]. The online parameter identification and SOC prediction are

investigated by equivalent modeling and altering the decoupled least-squares method to establish an improved model-based adaptive filter [56], [57]. OCV characterization is realized for various temperature levels of the forthcoming energy management of the battery system [58], and with the variation relationship of OCV versus SOC, the SOC inferred through the OCV-SOC table and identified parameters are input into the AEKF-based iterative calculation procedure to realize online capacity estimation.

To overcome the limitations of the traditional EKF method for SOC prediction, an improved multiple feature-electrochemical thermal coupling (MF-ETC) modeling and improved decoupled corrected deviation-extended Kalman filtering (DD-EKF) methods are proposed in this paper by considering the time-varying current and temperature influences. The main contributions of this paper are:

1) An improved multiple feature-electrochemical thermal coupling model is constructed. By exploring the dynamic characterization of multi-parameter coupling and functional relationships in battery models, a strategy to separate the internal characteristic impedance of batteries into short-term voltage changes caused by charge transfer and long-term voltage changes caused by diffusion effects is proposed.

2) An adaptive asynchronous parameter identification strategy is proposed for low-temperature environments. By separating and characterizing the lumped characteristic model parameters at different time scales, the prediction accuracy is improved across a wide range with real-time feedback correction.

3) A real-time estimation strategy of battery SOC based on decoupled deviation-extended Kalman filtering is proposed. Improved modeling equations are established for the SOC prediction using the Gaussian trinomial function, which is adaptive to the time-varying factors and can reduce the cumulative error caused by current in the traditional calculation formula. Online parameter identification and SOC prediction are investigated by equivalent modeling and altering the decoupled least-squares method to establish an improved model-based adaptive filter.

The remaining sections of this paper are organized as follows: In Section II, the mathematical analysis is conducted to establish the improved MF-ETC modeling method with high-precision advantages. In Section II.A, impedance elements are introduced to improve prediction accuracy. Then, the improved DD-EKF prediction method is described in detail in Section II.B, which is then introduced into the iterative calculation in Section II.C. In Section III, the experimental test results are given. The testing platform is designed in Section III.A with detailed model parameter identification. The sensitivity of each parameter is analyzed in detail in Section III.B. Subsequently, the complex experimental analysis

is described in Sections III.C and III.D with the noise-influencing coefficient correction (NICC), Beijing bus dynamic stress test (BBDST), and dynamic stress test (DST) conditions. The accuracy and robustness of the proposed methods are verified under the NICC and complex conditions. Section IV is the conclusion, which analyzes the research achievements and some related future research perspectives.

Highlights:

1) Electrochemical-thermal-coupling modeling for multi-dimensional factor extraction.

2) Parameter influence characterization with a multi-variable coupling relationship.

3) Decoupled corrected deviation-extended Kalman filtering for adaptive calculation.

4) Optimized battery state of charge prediction with real-time fractional feedback correction.

5) Complex BBDST and DST condition tests with a max error of 4.57% and 0.223%.

II. MATHEMATICAL ANALYSIS

A. Multi-parameter Coupling and Dynamic Numerical Characterization of Functional Relationship

In this subsection, the change law of key parameters is obtained by a multi-condition simulation together with the mapping relationship. The optimization mechanism of feature extraction is revealed, and the mathematical representation of the multi-parameter coupling relationship in the carrier transport process is explored with accuracy verification. Based on the numerical characterization of the complex condition influence, the cooperative transport mechanism of carriers between electrode materials is investigated as well as the output parameters and various characteristics of the batteries. The main factors influencing output performance are extracted together with their logical relationship, obtaining the variation law of the model parameters under the influence of different conditions. The mathematical descriptions and characteristic parameter identification process are designed for the variation law of core factors with various characteristics together with the variation law of model parameters.

To solve the problem of multi-parameter coupling and functional relationship characterization, the research mechanism is constructed from physical phenomena for the essential feature information extraction and mathematical description. Three research aspects are carried out, including the carrier cooperation mechanism between positive-negative electrodes and electrolytes, feature information extraction and behavior description under complex low-temperature conditions, and the changing law characterization of core factors affecting low-temperature characteristics. The carrier coordination mechanism is conducted between the positive and negative electrodes, and electrolytes based on dynamic modeling. The internal mechanism of

lithium-ion batteries is analyzed to clarify their dynamic characteristics in low-temperature conditions. The cooperative carrier transport mechanism is obtained between electrode materials by considering the decisive role of temperature in the carrier transport process. That process is described as: 1) The solid-phase diffusion in the cathode material lattice is investigated. 2) The charge transfer of lithium ions is analyzed through the cathode-electrolyte interface. 3) The solvation process occurs when lithium ions enter the electrolyte. 4) Liquid phase migration takes place for solvated clusters. 5) The desolvation of lithium ions occurs at the negative electrode-electrolyte interface. 6) The lithium ions pass through the negative SEI layer. 7) The solid-phase diffusion of lithium ions between anode material layers. The influence of low-temperature conditions on the carrier transport process in each step is considered, especially the significant attenuation of low-temperature dynamic performance.

The difficulty of improving low-temperature battery performance is to accurately judge the speed-limiting link in the carrier transport process. This is used to carry out multi-component and multi-strategy collaborative optimization together with the physical essence. Through element doping and heterogeneous interface construction, the transmission path of lithium ions in electrode materials is widened. After that, the diffusion rate in the solid-state electrode is accelerated. High

conductivity components are added to construct a fast coordinated ion transport channel to accelerate the charge transport process of electrolytes in complex structures. The multi-component electrode material is used to express the interface characteristics, and a local potential field is constructed to reduce the interface reaction barrier and accelerate the interface mass transfer in the load transfer process. By interface regulation, the side reactions are restrained. Consequently, loss of battery capacity is avoided with safety insurance. The effects of different optimization strategies are analyzed on the key behavior characteristics of batteries in low-temperature conditions to identify the main influence process.

In view of the random and dynamic characteristics of energy supply, the input and output characteristics in different working conditions are fully considered. External characteristics are analyzed to obtain the change patterns of key parameters such as open circuit voltage, closed circuit voltage (CCV), current multiplication rate, SOC, ageing degree, internal resistance and temperature through experiment. By exploring the main influencing factors of output performance and their logical relationships, static and dynamic response functions are established to realize the feature extraction and behavioral description of input and output data in different working conditions at extreme low temperatures, as shown in Fig. 1.

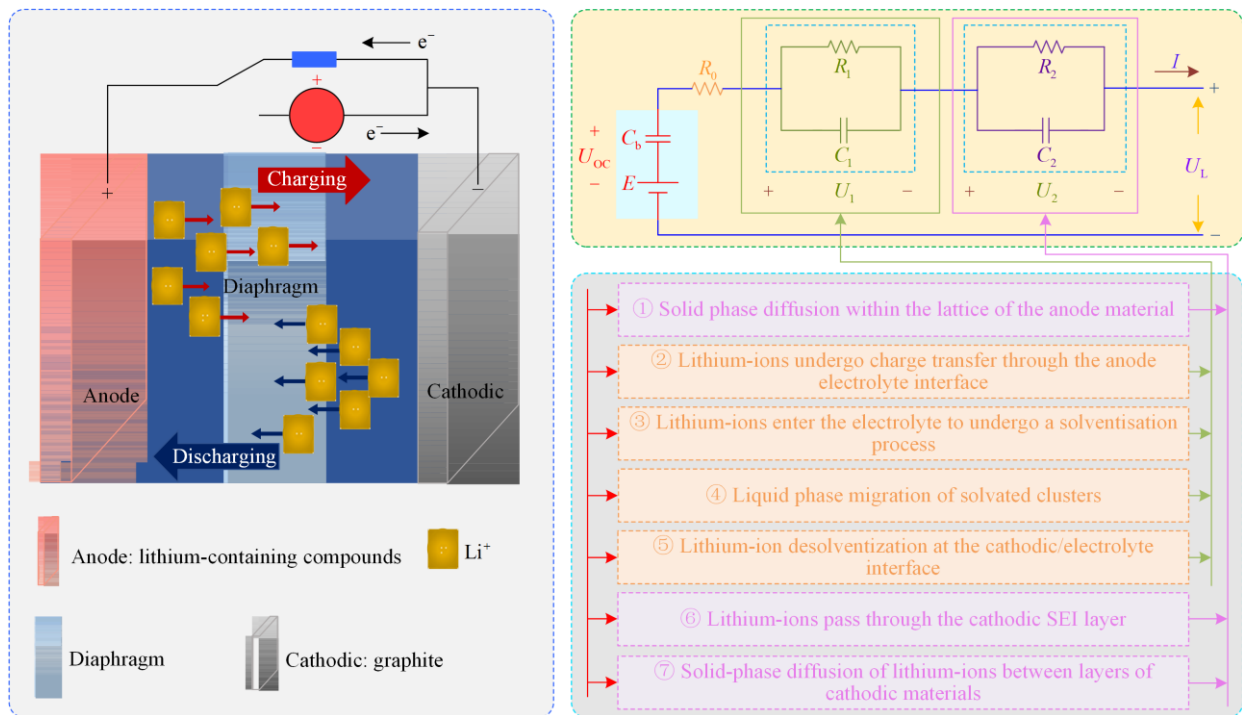


Fig. 1. Feature extraction and behavioral description under different working conditions at extreme low temperature.

As shown in Fig. 1, based on experimental data and circuit methods, the carrier transport process is simulated, and the relationship between aging effect, performance attenuation, and characteristic parameters is

analyzed to mathematically express the relationship between internal parameters and battery performance. The charge transfer of lithium ions through the anode/electrolyte interface, the Solvation process of lith-

ium ions entering the electrolyte, the liquid phase migration of solvation clusters, and the desolvation of lithium ions at the cathode/electrolyte interface are characterized as load transfer resistance R_1 and double layer capacitance C_1 . Modeling and characterizing the solid phase diffusion inside the positive electrode material lattice, lithium ion diffusion through the negative SEI layer, and lithium ion solid phase diffusion between the negative electrode material layers as diffusion resistance R_2 and diffusion capacitance C_2 , it further achieves accurate description of input and output behavior characteristics under extreme low temperature and complex working conditions. The model is improved by introducing the influence noise of complex working conditions, describing the functional relationship between parameters and expression of the state equation. The mathematical description of the operating characteristics is obtained by considering the effects of capacity degradation and temperature, combined with the analysis of simulated operating conditions, and a dynamically adaptable state space description of the external characteristics of the battery is established as:

$$\begin{cases} \frac{dU_1}{dt} = \frac{I_t}{C_1} - \frac{U_1}{R_1 C_1} \\ \frac{dU_2}{dt} = \frac{I_t}{C_2} - \frac{U_2}{R_2 C_2} \\ U_L = U_{OC}(SOC_t) - I_t R_0 - U_1 - U_2 \end{cases} \quad (1)$$

where U_i is equivalent polarization voltage; I_t is load current; R_0 is internal resistance of the battery; U_{OC} is open circuit voltage of the battery and U_L is terminal voltage. To eliminate the randomness trend contained in the data sequence, equation (1) is reduced and discretization by first-order reverse difference, and the discrete state space expression can be obtained as:

$$\begin{cases} [U_1(k) - U_1(k-1)]/T = \\ \quad -U_1(k)/RC + I(k)/C_1 \\ [U_1(k-1) - U_1(k-2)]/T = \\ \quad -U_1(k-1)/R_1 C_1 + I(k-1)/C_1 \\ [U_2(k) - U_2(k-1)]/T = \\ \quad -U_2(k)/R_2 C_2 + I(k)/C_2 \\ [U_2(k-1) - U_2(k-2)]/T = \\ \quad -U_2(k-1)/R_2 C_2 + I(k-1)/C_2 \end{cases} \quad (2)$$

To further reduce computational complexity, a parameter matrix $[c_1 \ c_2 \ c_3 \ c_4 \ c_5]$ is introduced to simplify (2) as:

$$U_L(k) = c_0 + c_1 U_L(k-1) + c_2 U_L(k-2) + c_3 I(k) + c_4 I(k-1) + c_5 I(k-2) \quad (3)$$

where the coefficients $[c_1 \ c_2 \ c_3 \ c_4 \ c_5]$ are the parameters that need to be identified in the discrete

system. According to the bilinear variation of the system, the relationship between discrete system parameters and equivalent circuit model parameters is:

$$\rho = \begin{bmatrix} R_0 \\ R_1 \\ R_2 \\ C_1 \\ C_2 \end{bmatrix} = \begin{bmatrix} \frac{c_5}{c_2} \\ \left\{ \left[-\tau_1 \frac{c_3 + c_4 + c_5}{1 - c_1 - c_2} + R_0 \frac{c_1 + 2c_2}{1 - c_1 - c_2} T - \right. \right. \\ \left. \left. R_0 \tau_1 - \frac{c_4 + 2c_5}{1 - c_1 - c_2} T \right] / (\tau_1 - \tau_2) \right\} \\ -\frac{c_3 + c_4 + c_5}{1 - c_1 - c_2} - R_0 - R_1 \\ \frac{\tau_1}{R_1} \\ \frac{\tau_2}{R_2} \end{bmatrix} \quad (4)$$

where $\tau_1 = R_1 C_1$, and $\tau_2 = R_2 C_2$. According to the system discrete expression shown in (3), a multi-feature least squares expression for the battery external characteristic model in the discrete domain can be constructed and parameter identification can be carried out. A real-time prediction model for multi-feature parameters can be established as:

$$\begin{cases} \mathbf{G}(k) = \mathbf{P}(k-1)\boldsymbol{\varphi}(k) \\ \quad [I_{n_p} + \boldsymbol{\varphi}^T(n_p, k)\mathbf{P}(k-1)\boldsymbol{\varphi}(n_p, k)]^{-1} \\ \mathbf{P}(k) = \mathbf{P}(k-1) - \\ \quad \mathbf{G}(k)\boldsymbol{\varphi}^T(k)\mathbf{P}(k-1) \\ \hat{\theta}(k) = \hat{\theta}(k-1) + \\ \quad \mathbf{G}(k)[\mathbf{Y}(k) - \boldsymbol{\varphi}^T(k)\hat{\theta}(k-1)] \end{cases} \quad (5)$$

where $\hat{\theta}(k)$ are the parameters to be identified for discrete systems; $\boldsymbol{\varphi}(k)$ is a data vector in a discrete system; $\boldsymbol{\varphi}^T(k)\hat{\theta}(k-1)$ is the system observation value at the previous time; $\mathbf{P}(k)$ is the error covariance matrix of the system; $\mathbf{Y}(k)$ is the system output multiple innovation matrix; and $\mathbf{G}(k)$ is the system real-time gain matrix. The difference between the calculated and actual observed values of the system observations, as well as the system gain, are used to correct the final estimate.

An accurate mathematical description is conducted for the main factor variation law that affects the characteristics. The mathematical description procedure of the key-factor changing law is designed to reduce the characterization error caused by the multi-information combination treatment in the cooperative carrier transport processes. The characteristics of voltage, internal resistance, temperature, and self-discharge effect are also analyzed. The dynamic varying law is explored

for CCV towards the current magnification and temperature variation. Then the mathematical description is obtained for the correlation between capacity attenuation, internal resistance increase, and output characteristics. The description mechanism is clarified for the battery charge-discharge processes to obtain the quantitative speed mismatch characterization of the chemical

reaction processes. These processes include internal charge transfer, electric double-layer effect, and carrier diffusion in solid particles. The multi-time-scale effect inside the battery is then described. The core factor variation law of characteristics is analyzed by designing an accurate mathematical description and parameter identification process, as shown in Fig. 2.

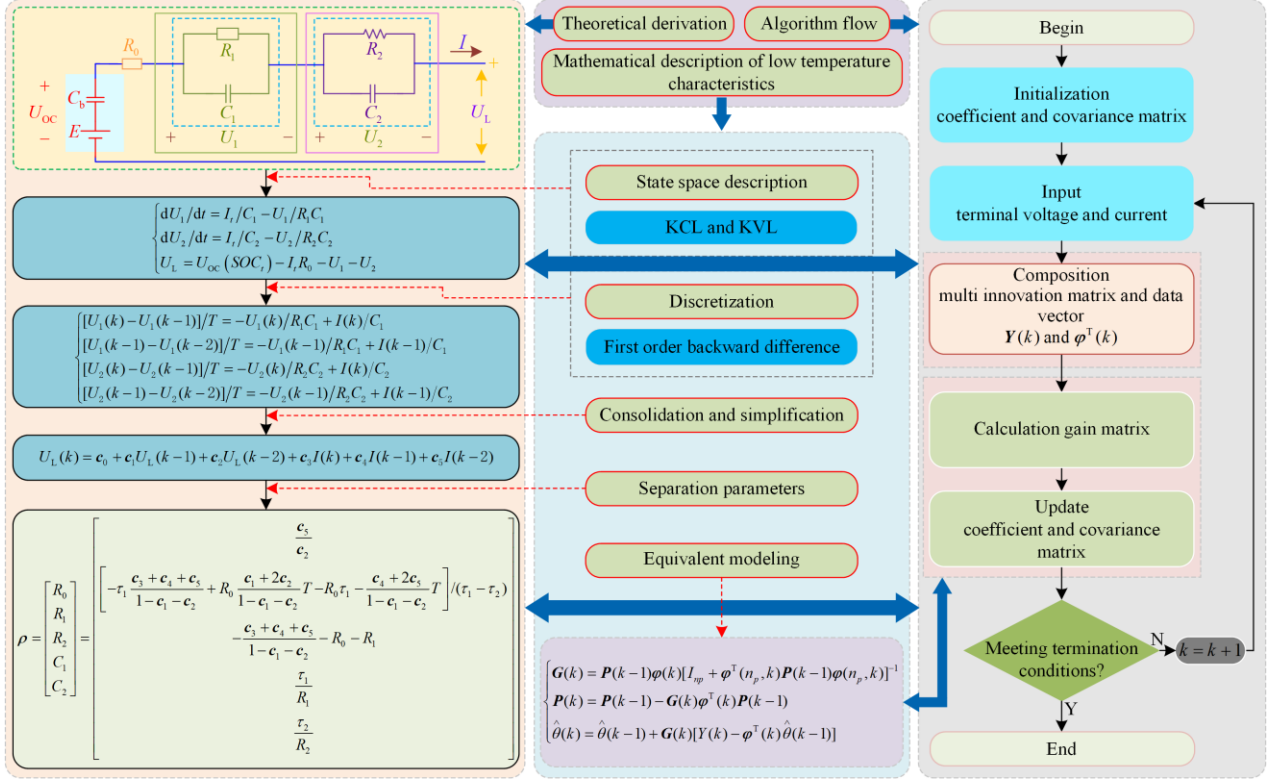


Fig. 2. Accurate description of mathematical characteristics and change process of key factors.

In Fig. 2, the expression effect of characteristics caused by the change of various parameters is analyzed. Then, the characteristic parameters are modified and the combined structure is optimized accordingly. Based on the mechanism analysis and dynamic description, the strategy of structural optimization and state representation is explored. This is used to improve the accuracy of parameter identification and accelerate the convergence effect of the algorithm. The characteristics of low-temperature batteries can then be described by partial least squares, polynomial fitting, and other algorithms. Subsequently, the innovative battery characteristics in low-temperature conditions are used for the iterative calculation to complete the accurate expression of different characteristics. By exploring the multi-dimensional mechanism of the internal and external battery characteristics in low-temperature conditions, the variation law of the key factors is obtained for describing the carrier transport process.

B. Compound Modeling of Low-temperature and Improvement Strategy of State-space Equations

A composite MF-ETC model is constructed by con-

sidering the mathematical description of dynamic characteristics. Combined with the state-space description, the accurate mathematical characteristics are expressed as well as the characteristic information extraction. Consequently, the state-space expression is used as the basis for rapid performance evaluation for extremely low-temperature lithium-ion batteries. Based on the self-recovery effect analysis of the battery capacity, the available capacity evaluation process is optimized by considering the action mechanism of unavailable charge at low temperature. The mathematical simulation of the carrier transport process is realized by the circuit-oriented and electrochemical-electrothermal supplementary design. The composite modeling characteristics are described for multi-time-scale conditions. Considering the low-temperature influence and the hysteretic OCV characteristics, the time-varying temperature characteristics are integrated to realize the structural design and optimization of the multi-time-scale battery characteristic model. The influencing factors are analyzed in different conditions, and a composite model framework is constructed. Combined

with the condition characterization analysis, the effect of each module is studied, and the combined structure is optimized by conducting various component combinations. By distinguishing the different external battery

characteristics under transient and steady-state conditions, the influence of the multi-time-scale effect is eliminated, and a structural optimization is realized for the electrical characteristic model, as shown in Fig. 3.

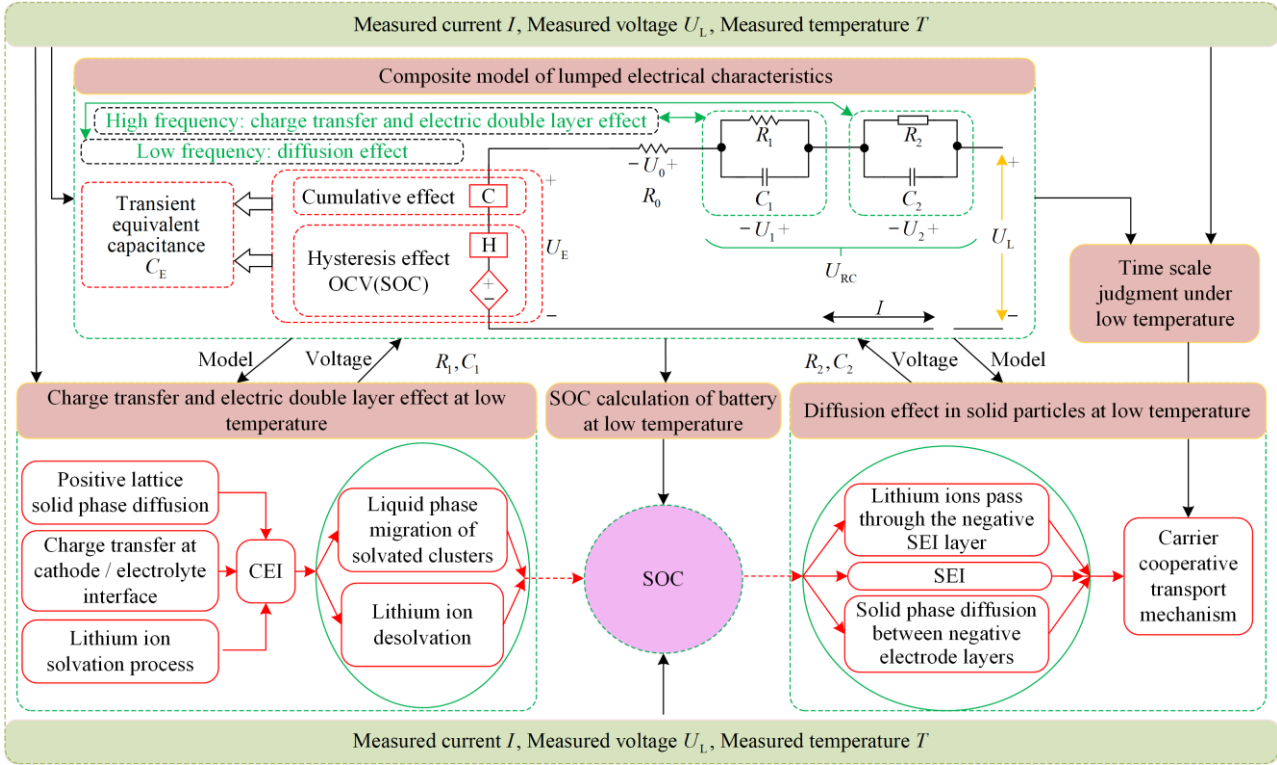


Fig. 3. Structure design and optimization of the multi-time-scale characteristic model of lithium-ion batteries.

In Fig. 3, the voltages at both ends of the module are fully represented by the voltage accumulation function in low-temperature conditions. The hysteresis function is represented by the voltages at both ends of the module in open circuit conditions. The impedance part includes ohmic, electrochemical polarization, and concentration polarization impedances. In the MF-ETC model, the ohmic impedance R_0 is mainly represented by the migration of lithium ions in the electrolyte, and is formed when electrons pass through the collector and electrolyte, so its volt-ampere characteristic relationship is represented by the transient voltage. The second-order RC network is used to describe the electrochemical and concentration polarization processes inside the battery, so its volt-ampere characteristic relationship is the slow change of voltage. For the charge transfer resistance R_1 and electric double layer capacitance C_1 in the electrochemical polarization impedance, they are mainly manifested in the solid-phase diffusion of the positive order lattice and the charge transfer at the electrolyte interface. The diffusion resistance R_2 and diffusion capacitance C_2 in the concentration polarization impedance mainly show the diffusion effect of lithium ions

through the SEI film and interlayer solid particles. The dynamic cooperative characterization of the carrier transport process in the positive, negative, and electrolyte of the battery is realized by electrical characteristic modeling in low-temperature conditions.

C. Adaptive Asynchronous Model Parameter Identification Under Low-temperature Conditions

Using the established characteristic model for the strong-applicability lithium-ion batteries, the multi-time-scale asynchronous parameter identification framework is designed. The adaptive model parameter online identification strategy is constructed. Based on the numerical characterization of the complex condition influence, the mathematical characterization is explored for the coupling relationship among multiple parameters. Consequently, the variation characteristics of output parameters in different conditions are fully considered. The variation law of the model parameters is obtained taking account of the influence of different current magnifications, pressure, aging, and temperature conditions. At low temperature, the battery voltage response for variable current includes both fast response and slow change. In addition, the dynamic battery characteristics are distributed over a wide frequency range. Thus, the above problems greatly affect the accuracy of model parameter identification, and may even lead to oscilla-

tion or divergence of identification results. In addition, as the structural complexity of the model increases, the identification of all parameters over the same time scale increases the amount of calculation and aggravates the difficulty of generation of the ill-conditioned matrix.

Therefore, the framework structure of adaptive multi-time-scale asynchronous parameter identification is designed to effectively solve the poor robustness problem caused by the single-time-scale parameter identification, as shown in Fig. 4.

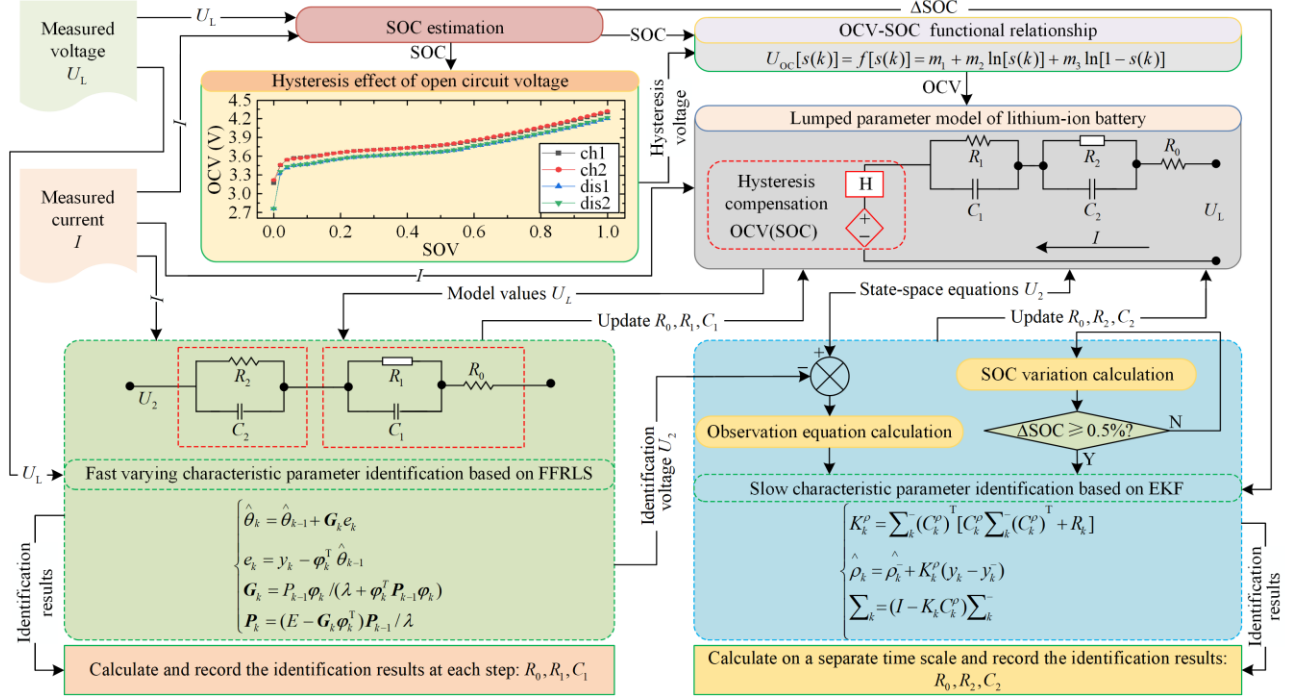


Fig. 4. The framework structure of adaptive multi-timescale asynchronous parameter identification.

As shown in Fig. 4, the full parameter identification accuracy is improved at different steps by constructing an adaptive asynchronous parameter identification strategy. It is realized by combining the forgetting factor recursive least squares (FFRLS) and EKF algorithms. This is also combined with the correction method affected by the dual effects of time-varying hysteresis. The EKF algorithm is introduced to preprocess the model parameters at low frequencies. This is used to improve the model parameter identification strategy at different frequencies to efficiently characterize the carrier transport process and electric double layer effect in lithium-ion batteries. By analyzing the transmission mechanism of carriers in batteries, the long-time-scale starting conditions are designed into the adaptive asynchronous identification strategy. Considering the uncertainty of conditions and the multi-time-scale influence effect, the SOC change is taken as the judgment condition of long-time constant identification. Considering the changing magnitude and current direction, the starting time point of the designed algorithm is not limited by the fixed high-frequency identification condition of the FFRLS. Compared with the judgment condition of fixed large step size, this judgment method can make the asynchronous identification algorithm adapt to a variety of current conditions, thereby improving the parameter identification accuracy, reducing the com-

putational complexity, and improving the consistency of model parameter identification.

D. Decoupled Deviation-extended Kalman Filtering

For an accurate prediction-correction process, an improved DD-EKF prediction model is constructed in real-time conditions. This produces an accurate SOC prediction of lithium-ion batteries to avoid destructive emanating factors. An observation update is conducted with the iterative calculation. This is then used for the state variable prediction. The time and measurement update steps are realized when introduced into the iterative SOC prediction and updating processes, providing an a priori sequence point prediction of the next time point. It is imposed on the state prediction procedure at the last time point. Consequently, the effective iterative calculation of the DD-EKF method is designed and realized, as shown in Fig. 5.

In Fig. 5, the calculation procedure undergoes two-stage calculation steps suitable for both static and dynamic periods. The SOC prediction is investigated as it is involved in the calculation process. With more detailed records of the prediction results for each iteration step, the Jacobian matrix is recalculated with the update step. The prediction method is performed iteratively with the correction and update being accumulated. Compared with other methods, the DD-EKF method is

simpler to apply in various conditions to obtain robust and accurate predictions. From the calculation, the SOC prediction is derived and prepared for the remaining energy determination.

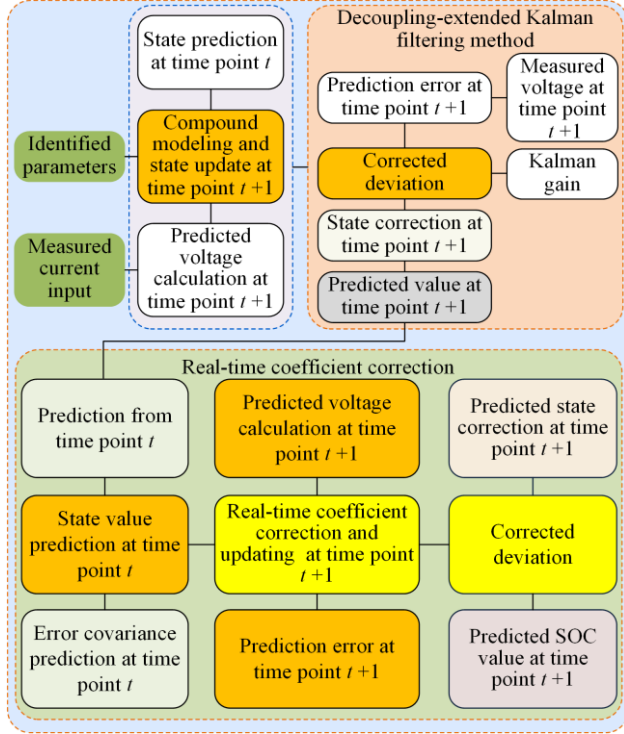


Fig. 5. The flowchart of the decoupled corrected deviation-extended Kalman filtering method.

E. Real-time Statistical Coefficient Correction

The dual ‘unscented’ transformation strategy is introduced to deal with nonlinear problems using a mathematical method whose fundamental principle is embedded in the iterative calculation process. The sampling points are obtained with the statistical characteristics of state variables using a data sampling strategy. The data acquisition is then combined with the sampling strategy and symmetric prediction-correction procedure. The overall research process for real-time prediction of the battery SOC is shown in Fig. 6.

As shown in Fig. 6, after obtaining the main parameters in the proposed MF-ETC model, the state-space equation is established with the relationship between voltage and current. The expectation and covariance are linearized during the state prediction process to obtain the observation equation, as:

$$y = h[x_t, I_t] + v_t = U_{OC} - R_0 I_t - U_{pt} + v_t \quad (6)$$

where y_{t+1} is the observation variable at the time point $t+1$; x_t is the state variable at the time point t ; I_t is the current at the time point t that is used as the input parameter; v_t is the observation noise; U_{OC} is the OCV value; R_0 is the ohmic resistance; and U_{pt} is the elec-

trochemical polarization voltage at the time point t . The unscented transformation is a suitable method to deal with nonlinear problems by considering the relationship between voltage and current after obtaining the main parameters in the equivalent model. Subsequently, the matrices A_t , B_t , and C_t are obtained as:

$$\begin{cases} A_t = \begin{bmatrix} 1 & 0 \\ 0 & e^{-\Delta t/\tau} \end{bmatrix} \\ B_t = \begin{bmatrix} -\Delta t/Q_n \\ R_p(1 - e^{-t/\tau}) \end{bmatrix} \\ C_t = \begin{bmatrix} \partial U_{OC} \\ \partial S \end{bmatrix} - 1 \end{cases} \quad (7)$$

where A_t is the state transition matrix at the time point t ; B_t is the control-input matrix at the time point t ; and C_t is the observation matrix at the time point t .

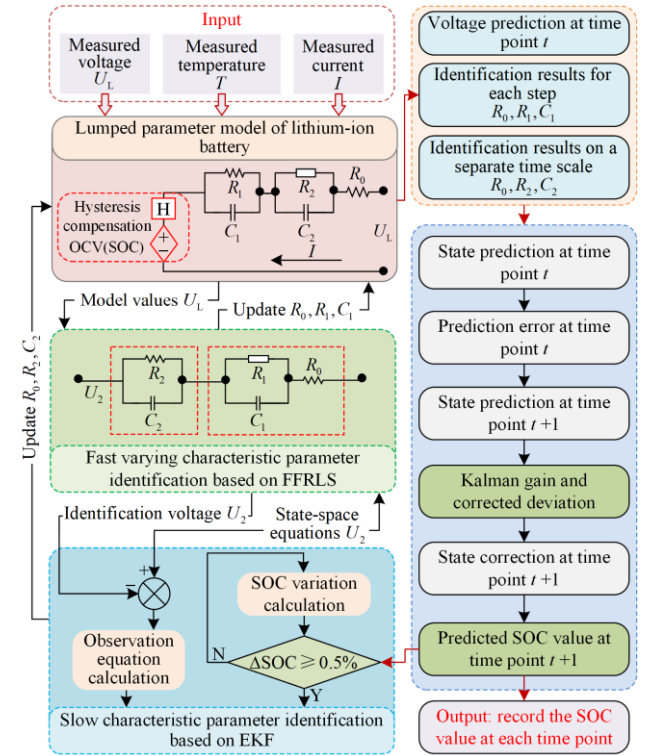


Fig. 6. Overall research flow chart of real-time prediction of battery SOC.

The first step is state prediction, in which SOC prediction is conducted using the state value at the last time point. The current and voltage parameters are easily measured directly in the real-time monitoring process. So the SOC prediction-correction process is investigated and represented for the iterative calculation. The calculation procedure is combined with the battery characteristics, and the predicted value is obtained as:

$$x_{t+1|t} = A_t x(t) + B_t I_t \quad (8)$$

where $x(t+1|t)$ is the state prediction value from the time point t to the time point $t+1$; A_t is the coefficient for the state parameter matrix $x(t)$ at the time point t ; and B_t is the control-input matrix for the input parameter I_t at the time point t .

The covariance prediction is investigated in the second step, where the precise value is obtained accordingly. By linearizing the estimated parameters, an accurate SOC prediction is achieved for lithium-ion batteries, performed by the linear Kalman filtering method. The error covariance matrix in the prediction step is calculated during the time update step as:

$$P_t^- = A_t P_t^+ A_t^T + \delta_t \quad (9)$$

where $P_{t+1|t}^-$ is the error covariance matrix in the prediction step at the time point t ; P_t^+ is the error covariance matrix at the time point t ; and δ_t is the system noise at the time point t . Therefore, an a priori prediction for the time point t is investigated. The mathematical model is established to be different from the value measured directly by the system because of the prediction process and measurement accuracy.

A third step is then conducted to obtain the feedback coefficient using measured parameters. The Kalman gain in the iterative calculation procedure is obtained:

$$K_t = P_t^- C_t^T (C_t P_t^- C_t^T + R_t)^{-1} \quad (10)$$

where K_t is the Kalman gain at the time point t ; and P_t^- is the error covariance matrix at the time point t .

The iterative SOC calculation scheme is designed to realize the state and matrix initialization. These three steps are recursively iterated, and the state prediction is updated continuously for the updated processing step. The parameters are initialized as $\beta \geq 0$ and $0.2 \leq \alpha \leq 1.0$. t is used as an auxiliary scale factor and λ is introduced to describe the scaling parameter. The sampling points are used to reverse the original state that is transferred into the calculation process:

$$y^i = f(x^i), \quad i = 0 \sim 2n \quad (11)$$

where i is the particle number, which varies from 0 to $2n$; while y^i and x^i are the particle values after and before the transformation, respectively. The mean and covariance values of the state parameters are calculated by conducting the transformation, which is realized by real-time measurement. The sampling points are predicted by investigating the one-step calculation. Then, sigma sampling points are updated by upper equations for the SOC prediction. In the actual measurement process, the current is measured directly. The iterative

SOC calculation is conducted with simple mathematical expressions as:

$$S = \frac{Q_t}{Q_n} \times 100\%; S_t = \frac{Q_{It}}{Q_{In}} \times 100\% \quad (12)$$

where S is the SOC value; Q_t is the remaining capacity; Q_n is the rated capacity; while S_t is the SOC value obtained corresponding to the current condition I , which is obtained by taking Q_{It} as the remaining electric quantity and Q_{In} as the rated capacity corresponding to the current condition I . For the continuous-time implementation process, a mathematical expression is obtained, as shown in the first part of (13), while the real-time implementation of the discrete-time SOC prediction is realized after the discretization processing method, as:

$$S(t) = S(0) - \int_0^t \frac{\eta_i I(t)}{Q_n} dt \Rightarrow S_{n+1} = S_n - \frac{\eta_i \Delta t}{Q_n} I_n \quad (13)$$

where $S(t)$ is the SOC value at the time point t with the corresponding discretized version of S_{n+1} ; η_i is the Coulombic efficiency for the current condition I ; and $I(t)$ is the current value at the time point t with the corresponding discretized version I_n . The discretized SOC prediction model is facilitated by the energy and safety controls of the battery system to realize the SOC prediction for a reliable application.

III. EXPERIMENTAL ANALYSIS AND DISCUSSION

A. Experimental Test Platform Design and Construction

The instruments comprise a charge-discharge tester, a temperature chamber, and other supporting experimental equipment to provide an ambient condition. The experimental test platform is shown in Fig. 7.

In Fig. 7, the experimental test platform is designed and embedded in an industrial personal computer (IPC) that is connected to the CT-4016-5V100A-NTFA charge-discharge tester via TCP/IP so that the signals of U/I/T are measured simultaneously. All test batteries are fixed in the chamber based on the time-varying temperature and current variations. As the model parameters vary with ambient temperature variations, the tests are conducted at an ambient temperature of 25°C. Meanwhile, the RPT test is conducted at temperatures of 0°C, 25°C, and 45°C with a current rate of 0.3 C, 1 C, and 2 C. Then, the varying-temperature model parameters are further improved and applied in the iterative calculation process based on the complex condition requirements.

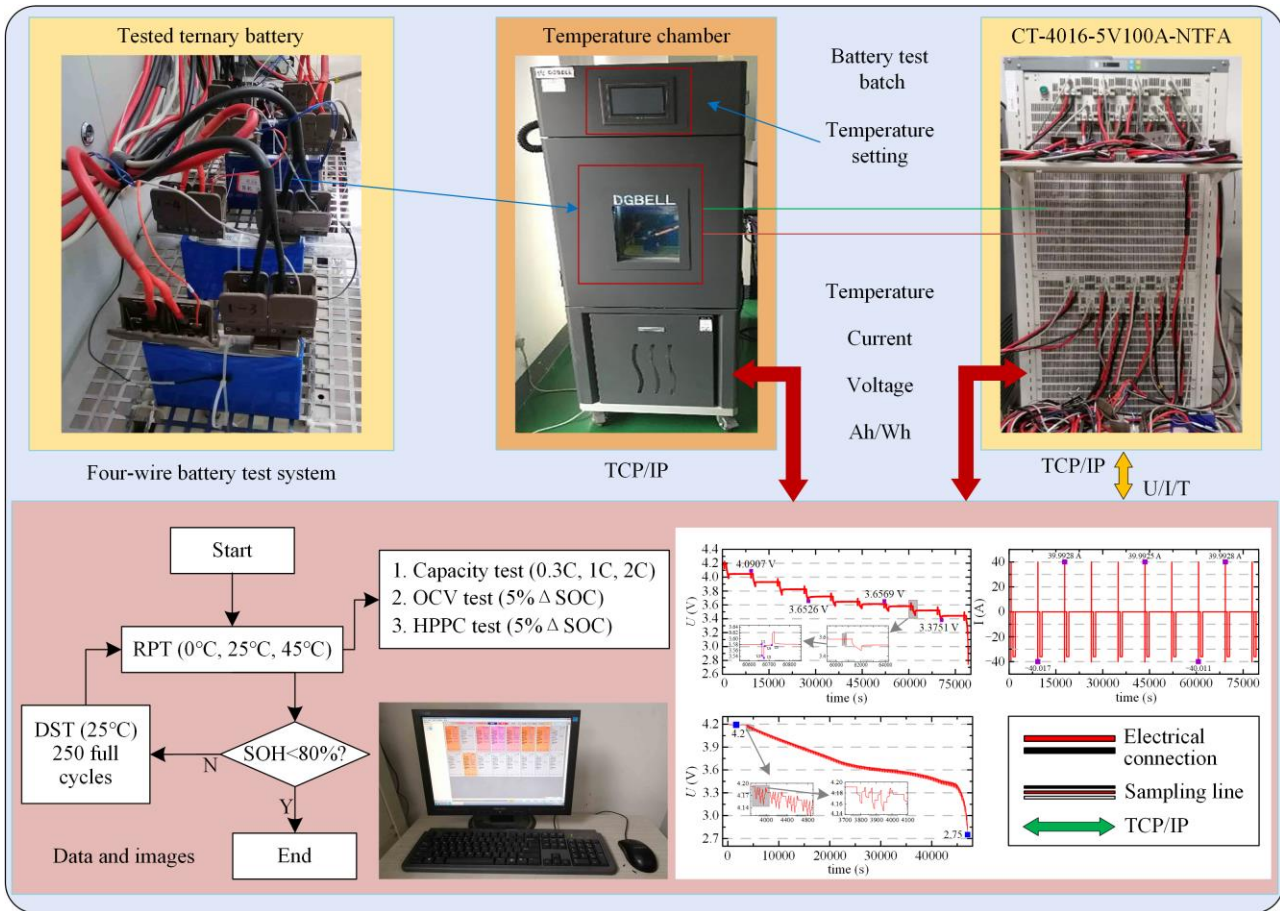


Fig. 7. The experimental test platform for the varying current rate and temperature tests.

B. Sensitivity Analysis

Researchs has shown that the parameters of the equivalent circuit model are crucial for improving the accuracy and stability of lithium-ion battery state estimation. All parameters in the equivalent circuit model are involved in the real-time update of SOC throughout the entire charging and discharging cycle, resulting in high computational costs. Therefore, it is necessary to conduct sensitivity analysis (SA) on model parameters to verify that model accuracy is improved without increasing model complexity and model parameter dimensions. On the other hand, it is possible to reduce the identification frequency of less sensitive parameters in the model and update the high sensitivity parameters in real-time to optimize calculation time and complexity, and reduce redundant estimation calculations.

The sensitivity of parameters is analyzed using the commonly used one-factor-at-a-time (OFAT) method. The basic idea of this method is to analyze the sensitivity of a certain parameter by changing the value of the parameter to an approximate normal value while retaining the values of other parameters, and then substituting these parameter values into the model to obtain the corresponding model error [59]. The parameter

sensitivity is reflected by the fluctuation of model error, and the higher the RMSE, the greater the parameter sensitivity. The parameter sensitivity of the MF-ETC model established in this paper based on the OFAT method is shown in Fig. 8.

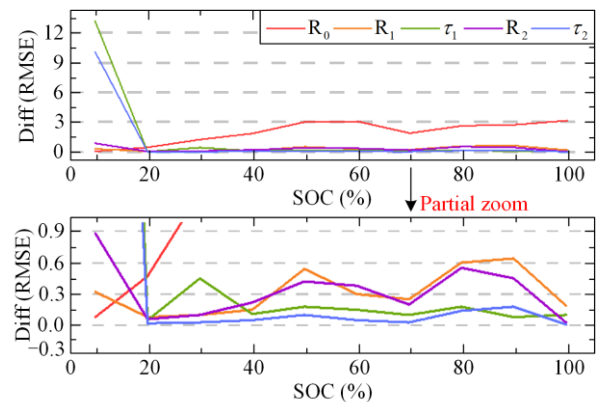


Fig. 8. Variation curve of model parameter sensitivity over the entire SOC range.

Figure 8 shows the derivative of the sensitivity of each model parameter within the entire SOC range of the battery, dynamically reflecting the stability of parameter sensitivity. As can be seen, the sensitivity of the

battery ohmic internal resistance R_0 is the highest and increases slowly as the SOC increases. This is followed by R_1 and R_2 , with R_1 being slightly more sensitive than R_2 in most cases. The weakest sensitivities are the time constants τ_1 and τ_2 , while τ_1 is more sensitive than τ_2 . The greatest variations in parameter sensitivity occur in the range of SOC $< 20\%$, and are caused by the inability of the equivalent model to accurately characterize the battery state at low SOC. When SOC $> 20\%$, the area of parameter sensitivity change is stable. The parameter sensitivities are evaluated qualitatively according to Fig. 8 and the results are summarized in Table II. The asterisk (★) indicates the sensitivity of the parameter, with more asterisks representing higher sensitivity.

TABLE II
SENSITIVITY ANALYSIS RESULTS OF MODEL PARAMETERS WITHIN THE ENTIRE SOC RANGE

Parameter	R_0	R_1	τ_1	R_2	τ_2
Sensitivity	★★★★★	★★★★★	★★	★★★★	★

It should be noted that sensitivity intensity is relative. It can be seen that the sensitivity of the RC loop in the MF-ETC model proposed in this paper is low. Thus, the identification frequency of these two parameters can be reduced to improve the accuracy of state estimation and reduce the computational cost, although they cannot be completely ignored. The reliability of the MF-ETC model adaptive asynchronous parameter identification method proposed in this paper has been verified.

C. Noise Influencing Coefficient Correction Effect

In the experimental tests, the proposed DD-EKF method is introduced for SOC prediction and verified at 0.5 C and 1.0 C constant-current (CC) discharging rates under high process and observation noise influences with the combined calculation equations. Based on the constructed MF-ETC model of lithium-ion batteries, the iterative calculation procedure is realized. The iterative DD-EKF method is expressed in the S -function to realize an accurate SOC prediction. In the complex BBDST condition, the SOC prediction results are verified by the experimental results, and the prediction effect is shown in Fig. 9.

In Fig. 9(a), the S1 curve is the actual SOC variation, and the S2 curve is the predicted SOC curve. The error results are analyzed in Fig. 9(b). From the experimental results, it can be observed that the maximum SOC prediction error is 3.87%. In the first 10 minutes, the maximum error is less than the overall maximum error value, because of the low discharge at this point. However, as the SOC decreases with increased discharge, it can be observed that the error increases but remains stable for the entire prediction process. This result shows the robustness of the proposed DD-EKF

method for SOC prediction. Compared with the SOC estimation results of the adaptive noise correction manual extended Kalman filtering proposed in [60] under the same conditions, the accuracy is improved by 1.07%, indicating that the algorithm proposed in this paper has better adaptability under strong noise conditions. However, the algorithm mentioned in [61] is applicable to a wider temperature range, while high temperature is not considered in this paper.

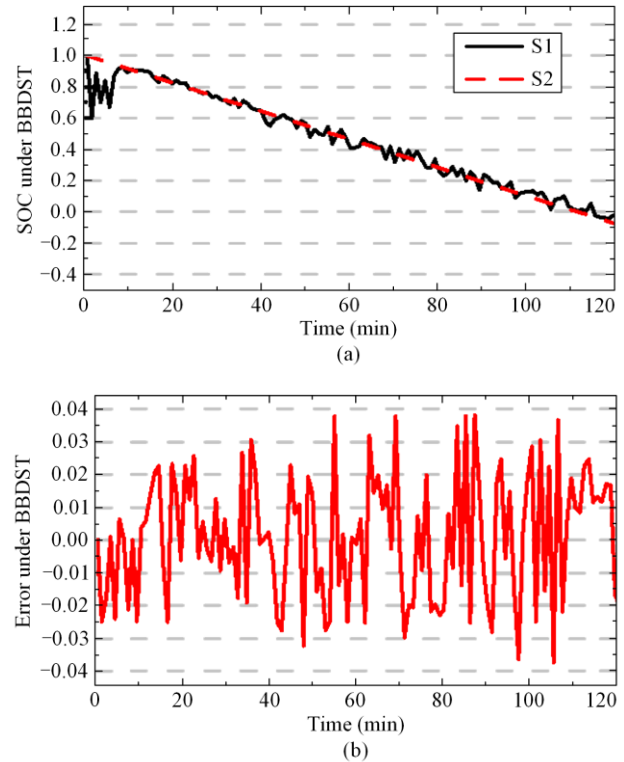


Fig. 9. SOC prediction effect with high noise effect under the BBDST condition. (a) SOC prediction curve for the BBDST condition. (b) Prediction error curve for the BBDST condition.

D. Complex Prediction Verification for the BBDST and DST Conditions

In complex conditions, the SOC prediction is investigated in both the BBDST and DST conditions to analyze the adaptability of the proposed DD-EKF method and compare it with the ampere-hour integration method. The tests results are shown in Fig. 10.

The variation of the input pulse power current variation is obtained in the BBDST condition, as shown in Fig. 10(a). Setting the initial SOC value to 0.75, the predicted SOC results are shown in Fig. 10(b), where S1 is the reference SOC of the system and S2 is the SOC predicted using the proposed DD-EKF method. From the errors in Fig. 10(c), it can be seen that the algorithm can track the reference SOC value of the battery in a short period of time, verifying its strong tracking performance. The method does not deviate from the initial phase and provides an accurate prediction compared with that in [61]. When the initial error is large, the

DD-EKF method is suitable for correcting the predicted error value. The robustness of the DD-EKF method for SOC prediction is further verified using the ampere-hour integration method in DST conditions. In Fig. 10(d), the input pulsed power current change predicted by SOC is obtained. The SOC prediction and its errors are shown in Figs. 10(e) and (f), respectively. In Fig. 10(e), S1 is the reference SOC value, S2 is the predicted value of the DD-EKF algorithm, and S3 is the SOC estimation result using ampere-hour integration. In Fig. 10(f), Err1 represents the estimation error of the DD-EKF, and Err2 represents the estimation error of the ampere-hour integration. It can be seen that the SOC prediction value of the proposed DD-EKF method converges to the actual value in a short time with a maximum error of 0.223%, while the SOC predicted through the ampere-hour integration method has a maximum error of 1.112%, verifying the strong robustness and accuracy of the algorithm. The maximum SOC prediction error values of the proposed DD-EKF method in BBDST and DST conditions are 4.57% and 0.223% respectively.

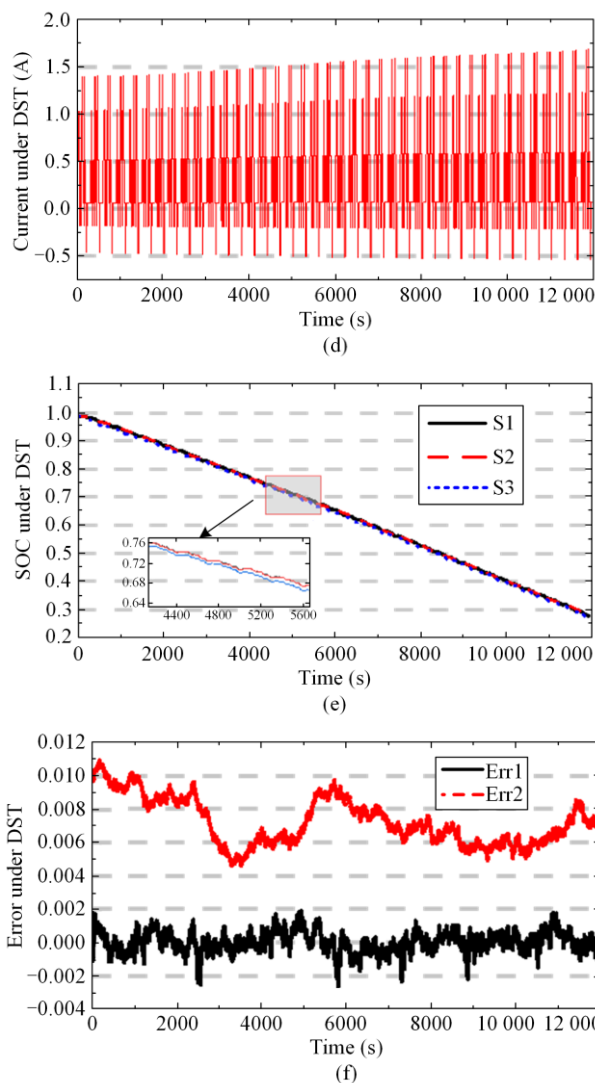
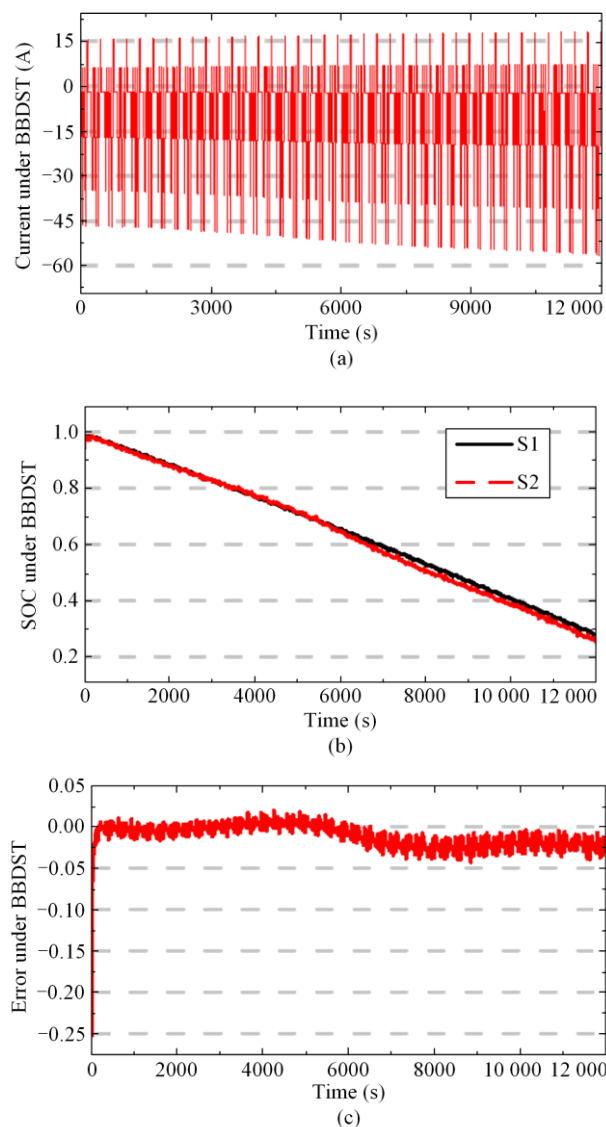


Fig. 10. The pulse power input current variation and SOC predictions in complex conditions. (a) The input pulse power current variation under the BBDST condition. (b) Real-time SOC prediction under the BBDST condition. (c) Prediction error under the BBDST condition. (d) The input pulse power current variation under the DST condition. (e) Real-time SOC prediction under the DST condition. (f) Prediction error under the DST condition.

From the prediction results, it can be seen that the proposed MF-ETC modeling and DD-EKF methods have stronger robustness than the traditional methods described in [62]. The SOC prediction of the iterative calculation method shows good experimental results from the pulse current variation, in which overall prediction error decreases and trends in the SOC prediction process of the small-scope fluctuation approach the actual value. The proposed methods overcome the accumulated error of the polarization effect. The proposed DD-EKF and MF-ETC modeling methods are applicable to the transient charge-discharge effect characterization and internal effect description, providing a new perspective on functional SOC prediction for lithium-ion batteries.

IV. CONCLUSION

SOC prediction is influenced by multiple internal parameters. In this paper, an improved multiple feature-electrochemical thermal coupling modelling method considering the frequency of parameter identification is proposed. It investigates the internal parameter inconsistencies of the battery, and is combined with an improved decoupled corrected deviation-extended Kalman filtering method for iterative SOC prediction and correction. The experimental results show that the maximum estimation error of SOC is only 3.87% under the influence of high process and observation noise. This indicates that the model correction coefficient is effective and can more accurately describe the high and low frequency dynamic characteristics of lithium-ion batteries than the traditional model, leading to more robust estimation results. The maximum SOC prediction errors of the proposed method are 4.57% and 0.223% in the BBDST and DST conditions, respectively, indicating effective initial value correction of the current and temperature variations. When the initial SOC value deviates, it can quickly track the actual value of the system, indicating its advantages of high precision and rapid regression, while considering the polarization effects and reducing the nonlinear effects. Accurate SOC prediction is realized to provide an effective way for accurate battery system modeling that is adaptive to the rational distribution of the internal parameters. The battery state prediction range is exceeded by reducing the divergence and linearization errors in complex conditions. It is noted that the method proposed in this paper has only been validated with experimental tests so needs to be further explored for real-world vehicle working conditions, while the effect of a wide temperature range on battery condition estimation also needs to be investigated.

ACKNOWLEDGMENT

Thanks to the sponsors. Carlos Fernandez also expresses his profound gratitude to Robert Gordon University for its support.

AUTHORS' CONTRIBUTIONS

Shunli Wang: draft, supervision, project management, conceptualization, and investigation. Haiying Gao: validation, data management, formal analysis, and writing. Paul Takyi-Aninakwa: project administration, review, and editing. Josep M. Guerrero: project administration and Funding acquisition. Carlos Fernandez: review and editing. Qi Huang: project management and investigation. All authors read and approved the final manuscript.

FUNDING

This work is supported by the National Natural Science Foundation of China (No. 62173281), the Natural

Science Foundation of Sichuan Province (No. 23ZDYF0734 and No. 2023NSFSC1436), and the Fund of Robot Technology Used for Special Environment Key Laboratory of Sichuan Province (No. 18kftk03).

AVAILABILITY OF DATA AND MATERIALS

Please contact the corresponding author for data material request.

DECLARATIONS

Competing interest: The authors declare that they have no known competing financial interests or personal relationships that could have appeared to influence the work reported in this article.

AUTHORS' INFORMATION

Shunli Wang received the M.Eng. degree in Detection Technology and Automation Device from Southwest University of Science and Technology, China in 2012, and the Ph.D. degree in Control Science and Engineering from Southwest University of Science and Technology, China in 2018. He is currently serving as an academic dean in the School of Electric Power, Inner Mongolia Institute of Technology University, and is a Top 2% Top Scientist in the world. His research interests include new energy and energy storage systems, green and low-carbon energy storage for smart grids.

Haiying Gao received her B.S. degree in Electrical Engineering and Automation from Southwest University of Science and Technology (SWUST) in 2017, and she is currently pursuing the M.Eng. degree in Electronics and Information at SWUST. From October 2023 to present, she has been working as the executive deputy director in the Smart Energy Storage Institute. Her research interests include new energy and energy storage system control, aging modeling and state estimation of lithium-ion power batteries.

Paul Takyi-Aninakwa received the M.S. degree in Mechanical Engineering from Southwest University of Science and Technology, China, in 2021, and he is currently pursuing the Ph.D. degree in Control Science and Engineering at Southwest University of Science and Technology, China. His research interests include lithium battery charge state and new energy measurement and control.

Josep M. Guerrero received the B.S. degree in telecommunications engineering, the M.S. degree in electronics engineering, and the Ph.D. degree in power electronics from the Technical University of Catalonia, Barcelona, in 1997, 2000 and 2003, respectively. Since 2011, he has been a full professor with the Department of Energy Technology, Aalborg University, Denmark,

where he is responsible for the microgrid research program. From 2012 he is a guest professor at the Chinese Academy of Science and the Nanjing University of Aeronautics and Astronautics; and from 2014 he is chair professor in Shandong University. His research interests include oriented to different microgrid aspects, including power electronics, distributed energy-storage systems, hierarchical and cooperative control, energy management systems, and optimization of microgrids and islanded minigrids.

Carlos Fernan-dez received Ph.D. degree in Electrocatalytic Reactions from The University of Hull (UK). He has been a lecturer in bioanalytical chemistry at Robert Gordon University since 2014. His research interests include analytical chemistry, sensors and materials and renewable energy.

Qi Huang received the M.S. degree in high voltage engineering from Tsinghua University in 1996, and the Ph.D. degree in electrical engineering from Arizona State University in 1999. He is currently the deputy secretary of the party committee and president of Southwest University of Science and Technology, and has been selected as an IEEE Fellow and an IET Fellow. His research interests include wide-area measurement and control of power systems, analysis and control of large power grids, information support technology for smart energy, grid-connected large-scale multiregenerative energy systems, and tunnel transmission.

REFERENCES

- [1] G. Chen, Z. Liu, and H. Su *et al.*, "Electrochemical-distributed thermal coupled model-based state of charge estimation for cylindrical lithium-ion batteries," *Control Engineering Practice*, vol. 109, pp. 1-11, Apr. 2021.
- [2] Y. Zheng, Z. Shi, and D. Guo *et al.*, "A simplification of the time-domain equivalent circuit model for lithium-ion batteries based on low-frequency electrochemical impedance spectra," *Journal of Power Sources*, vol. 489, pp. 1-12, Mar. 2021.
- [3] S. Zhou, X. Liu, and Y. Hua *et al.*, "Adaptive model parameter identification for lithium-ion batteries based on improved circuitry hybrid adaptive particle swarm optimization- simulated annealing method," *Journal of Power Sources*, vol. 482, pp. 1-12, Jan. 2021.
- [4] Z. Shuzhi, G. Xu, and Z. Xiongwen, "A novel one-way transmitted co-estimation framework for capacity and state-of-charge of lithium-ion battery based on double adaptive extended Kalman filters," *Journal of Energy Storage*, vol. 33, pp. 1-16, Jan. 2021.
- [5] X. Zhang, X. Sun, and X. Li *et al.*, "Recent progress in rate and cycling performance modifications of vanadium oxides cathode for lithium-ion batteries," *Journal of Energy Chemistry*, vol. 59, pp. 343-363, Aug. 2021.
- [6] K. Ando, T. Matsuda, and D. Imamura, "Degradation diagnosis of lithium-ion batteries using AC impedance technique in fixing the state of charge of an electrode," *Journal of Energy Chemistry*, vol. 53, pp. 285-289, May 2020.
- [7] C. Yan, Y. X. Yao, and W. L. Cai *et al.*, "The influence of formation temperature on the solid electrolyte interphase of graphite in lithium ion batteries," *Journal of Energy Chemistry*, vol. 49, pp. 335-338, Oct. 2020.
- [8] F. Mo, G. Liang, and Q. Meng *et al.*, "A flexible rechargeable aqueous zinc manganese-dioxide battery working at $-20\text{ }^{\circ}\text{C}$," *Energy & Environmental Science*, vol. 12, no. 2, pp. 706-715, Jan. 2019.
- [9] H. Ruan, B. Sun, and W. Zhang *et al.*, "Quantitative analysis of performance decrease and fast-charging limitation for lithium-ion batteries at low temperature based on the electrochemical model," *IEEE Transactions on Intelligent Transportation Systems*, vol. 22, no. 1, pp. 640-650, Jan. 2021.
- [10] C. Li, N. Cui, and C. Wang *et al.*, "Simplified electrochemical lithium-ion battery model with variable solid-phase diffusion and parameter identification over wide temperature range," *Journal of Power Sources*, vol. 497, no. 15, pp. 1-14, Jun. 2021.
- [11] H. You, H. Dai, and L. Li *et al.*, "Charging strategy optimization at low temperatures for li-ion batteries based on multi-factor circuitry aging model," *IEEE Transactions on Vehicular Technology*, vol. 70, no. 11, pp. 11433-11445, Sep. 2021.
- [12] J. Zhu, M. Knapp, and D.R. Sørensen *et al.*, "Investigation of capacity fade for 18650-type lithium-ion batteries cycled in different state of charge (SoC) ranges," *Journal of Power Sources*, vol. 489, pp. 1-12, Mar. 2021.
- [13] D. Wang, H. Huang, and Z. Tang *et al.*, "A lithium-ion battery electrochemical-thermal model for a wide temperature range applications," *Electrochimica Acta*, vol. 362, pp. 1-15, Dec. 2020.
- [14] Z. Ye and J. Yu, "State-of-health estimation for lithium-ion batteries using domain adversarial transfer learning," *IEEE Transactions on Power Electronics*, vol. 37, no. 3, pp. 3528-3543, Oct. 2022.
- [15] W. Wang, L.W. Fan, and P. Zhou, "Evolution of global fossil fuel trade dependencies," *Energy*, vol. 238, pp. 1-12, Jan. 2022.
- [16] Q. Zhang, L. Yang, and W. Guo *et al.*, "A deep learning method for lithium-ion battery remaining useful life prediction based on sparse segment data via cloud computing system," *Energy*, vol. 241, pp. 1-11, Feb. 2022.
- [17] Z. Ling, W. Lin, and Z. Zhang *et al.*, "Computationally efficient thermal network model and its application in optimization of battery thermal management system with phase change materials and long-term performance assessment," *Applied Energy*, vol. 259, pp. 1-9, Feb. 2020.
- [18] S. Wang, D. I. Stroe, and C. Fernandez *et al.*, "A novel energy management strategy for the ternary lithium batteries based on the dynamic equivalent circuit modeling and differential Kalman filtering under time-varying conditions," *Journal of Power Sources*, vol. 450, pp. 1-36, Feb. 2020.
- [19] Y. Tian, R. Lai, and X. Li *et al.*, "A combined method for state-of-charge estimation for lithium-ion batteries

- using a long short-term memory network and an adaptive cubature Kalman filter,” *Applied Energy*, vol. 265, pp. 1-14, May 2020.
- [20] J. Tian, R. Xiong, and W. Shen *et al.*, “Online simultaneous identification of parameters and order of a fractional order battery model,” *Journal of Cleaner Production*, vol. 247, pp. 1-14, Feb. 2020.
- [21] D. I. Stroe and E. Schaltz, “Lithium-ion battery state-of-health estimation using the incremental capacity analysis technique,” *IEEE Transactions on Industry Applications*, vol. 56, no. 1, pp. 678-685, Nov. 2020.
- [22] S. Greenbank and D. Howey, “Automated feature extraction and selection for data-driven models of rapid battery capacity fade and end of life,” *IEEE Transactions on Industrial Informatics*, vol. 18, no. 5, pp. 2965-2973, Aug. 2022.
- [23] X. Hu, H. Jiang, and F. Feng *et al.*, “An enhanced multi-state estimation hierarchy for advanced lithium-ion battery management,” *Applied Energy*, vol. 257, pp. 1-13, Jan. 2020.
- [24] L. Li, C. Wang, and S. Yan *et al.*, “A combination state of charge estimation method for ternary polymer lithium battery considering temperature influence,” *Journal of Power Sources*, vol. 484, pp. 1-17, Feb. 2021.
- [25] P. Shrivastava, T. K. Soon, and M. Y. I. B. Idris *et al.*, “Combined state of charge and state of energy estimation of lithium-ion battery using dual forgetting factor-based adaptive extended Kalman filter for electric vehicle applications,” *IEEE Transactions on Vehicular Technology*, vol. 70, no. 2, pp. 1200-1215, Jan. 2021.
- [26] T. Mesbahi, N. Rizouq, and P. Bartholomeus *et al.*, “Dynamic model of li-ion batteries incorporating electrothermal and ageing aspects for electric vehicle applications,” *IEEE Transactions on Industrial Electronics*, vol. 65, no. 2, pp. 1298-1305, Jun. 2018.
- [27] A. Barai, K. Uddin, and W.D. Widanage *et al.*, “A study of the influence of measurement timescale on internal resistance characterisation methodologies for lithium-ion cells,” *Scientific Reports*, vol. 8, no. 1, pp. 1-13, Jan. 2018.
- [28] B. Fridholm, T. Wik, and M. Nilsson, “Robust recursive impedance estimation for automotive lithium-ion batteries,” *Journal of Power Sources*, vol. 304, pp. 33-41, Feb. 2016.
- [29] X. Feng, C. Weng, and M. Ouyang *et al.*, “Online internal short circuit detection for a large format lithium ion battery,” *Applied Energy*, vol. 161, pp. 168-180, Jan. 2016.
- [30] M. Bruch, L. Millet, and J. Kowal *et al.*, “Novel method for the parameterization of a reliable equivalent circuit model for the precise simulation of a battery cell's electric behavior,” *Journal of Power Sources*, vol. 490, pp. 1-16, Apr. 2021.
- [31] G. P. Fenner, L.W. Stringini, and C.A. Rangel *et al.*, “Comprehensive model for real battery simulation responsive to variable load,” *Energies*, vol. 14, no. 11, pp. 1-18, May 2021.
- [32] R. Xiong, L. Li, and Q. Yu *et al.*, “A set membership theory based parameter and state of charge co-estimation method for all-climate batteries,” *Journal of Cleaner Production*, vol. 249, pp. 1-14, Mar. 2020.
- [33] Z. Wei, G. Dong, and X. Zhang *et al.*, “Noise-immune model identification and state-of-charge estimation for lithium-ion battery using bilinear parameterization,” *IEEE Transactions on Industrial Electronics*, vol. 68, no. 1, pp. 312-323, Jan. 2021.
- [34] Y. Zhou, M. Huang, and M. Pecht, “Remaining useful life estimation of lithium-ion cells based on k-nearest neighbor regression with differential evolution optimization,” *Journal of Cleaner Production*, vol. 249, pp. 1-12, Mar. 2020.
- [35] D. J. Xuan, Z. Shi, and J. Chen *et al.*, “Real-time estimation of state-of-charge in lithium-ion batteries using improved central difference transform method,” *Journal of Cleaner Production*, vol. 252, pp. 1-14, Apr. 2020.
- [36] D. Zhou, W. Zheng, and P. Fu *et al.*, “Research on online estimation of available capacity of lithium batteries based on daily charging data,” *Journal of Power Sources*, vol. 451, pp. 1-16, Mar. 2020.
- [37] C. Zheng, Z. Chen, and D. Huang, “Fault diagnosis of voltage sensor and current sensor for lithium-ion battery pack using hybrid system modeling and unscented particle filter,” *Energy*, vol. 191, pp. 1-13, Jan. 2020.
- [38] Y. Song, D. Liu, and H. Liao *et al.*, “A hybrid statistical data-driven method for on-line joint state estimation of lithium-ion batteries,” *Applied Energy*, vol. 261, pp. 1-13, Mar. 2020.
- [39] K.V. Singh, H.O. Bansal, and D. Singh, “Hardware-in-the-loop Implementation of ANFIS based adaptive SoC estimation of lithium-ion battery for hybrid vehicle applications,” *Journal of Energy Storage*, vol. 27, pp. 1-18, Feb. 2020.
- [40] J.Q. Huang, X. Lin, and H. Tan *et al.*, “Realizing high-performance Zn-ion batteries by a reduced graphene oxide block layer at room and low temperatures,” *Journal of Energy Chemistry*, vol. 43, pp. 1-7, Apr. 2020.
- [41] L. Yu, Q. Liu, and L. Wang *et al.*, “Boosting lithium batteries under harsh operating conditions by a resilient ionogel with liquid-like ionic conductivity,” *Journal of Energy Chemistry*, vol. 62, pp. 408-414, Nov. 2021.
- [42] M. Rana, B. Luo, and M. R. Kaiser *et al.*, “The role of functional materials to produce high areal capacity lithium sulfur battery,” *Journal of Energy Chemistry*, vol. 42, pp. 195-209, Mar. 2020.
- [43] C. Zhu, Y. Shang, and F. Lu *et al.*, “Core temperature estimation for self-heating automotive lithium-ion batteries in cold climates,” *IEEE Transactions on Industrial Informatics*, vol. 16, no. 5, pp. 3366-3375, Dec. 2020.
- [44] S. Randau, D.A. Weber, and O. Kötz *et al.*, “Benchmarking the performance of all-solid-state lithium batteries,” *Nature Energy*, vol. 5, no. 3, pp. 259-270, Mar. 2020.
- [45] Z. Chen, J. Zhou, and F. Zhou *et al.*, “State-of-charge estimation of lithium-ion batteries based on improved H infinity filter algorithm and its novel equalization method,” *Journal of Cleaner Production*, vol. 290, pp. 1-15, Mar. 2021.
- [46] H. Shi, S. Wang, and C. Fernandez *et al.*, “Improved multi-time scale lumped thermoelectric circuitry modeling and parameter dispersion evaluation of lithium-ion batteries,” *Applied Energy*, vol. 324, pp. 1-28, Oct. 2022.

- [47] Y. Xie, W. Li, and X. Hu *et al.*, "Novel mesoscale electrothermal modeling for lithium-ion batteries," *IEEE Transactions on Power Electronics*, vol. 35, no. 3, pp. 2595-2614, Jul. 2020.
- [48] Y. Wang, G. Gao, and X. Li *et al.*, "A fractional-order model-based state estimation approach for lithium-ion battery and ultra-capacitor hybrid power source system considering load trajectory," *Journal of Power Sources*, vol. 449, pp. 1-12, Feb. 2020.
- [49] S. Yang, C. Zhang, and J. Jiang *et al.*, "A voltage reconstruction model based on partial charging curve for state-of-health estimation of lithium-ion batteries," *Journal of Energy Storage*, vol. 35, pp. 1-15, Mar. 2021.
- [50] D. Sun, X. Yu, and C. Wang *et al.*, "State of charge estimation for lithium-ion battery based on an intelligent adaptive extended Kalman filter with improved noise estimator," *Energy*, vol. 214, pp. 1-14, Jan. 2021.
- [51] F. Xiao, C. Li, and Y. Fan *et al.*, "State of charge estimation for lithium-ion battery based on Gaussian process regression with deep recurrent kernel," *International Journal of Electrical Power & Energy Systems*, vol. 124, pp. 1-15, Jan. 2021.
- [52] S. Shen, M. Sadoughi, and M. Li *et al.*, "Deep convolutional neural networks with ensemble learning and transfer learning for capacity estimation of lithium-ion batteries," *Applied Energy*, vol. 260, pp. 1-14, Feb. 2020.
- [53] X. Qiu, W. Wu, and S. Wang, "Remaining useful life prediction of lithium-ion battery based on improved cuckoo search particle filter and a novel state of charge estimation method," *Journal of Power Sources*, vol. 450, pp. 1-13, Feb. 2020.
- [54] X. Lai, L. He, and S. Wang *et al.*, "Co-estimation of state of charge and state of power for lithium-ion batteries based on fractional variable-order model," *Journal of Cleaner Production*, vol. 255, pp. 1-14, May 2020.
- [55] K. Jiang, X. Liu, and G. Lou *et al.*, "Parameter sensitivity analysis and cathode structure optimization of a non-aqueous Li-O₂ battery model," *Journal of Power Sources*, vol. 451, pp. 1-11, Mar. 2020.
- [56] Z. Xia and J.A.A. Qahouq, "State-of-charge balancing of lithium-ion batteries with state-of-health awareness capability," *IEEE Transactions on Industry Applications*, vol. 57, no. 1, pp. 673-684, Oct. 2021.
- [57] C. Jiang, S. Wang, and B. Wu *et al.*, "A state-of-charge estimation method of the power lithium-ion battery in complex conditions based on adaptive square root extended Kalman filter," *Energy*, vol. 219, pp. 1-11, Mar. 2021.
- [58] Z. Chen, L. Chen, and W. Shen *et al.*, "Remaining useful life prediction of lithium-ion battery via a sequence decomposition and deep learning integrated approach," *IEEE Transactions on Vehicular Technology*, vol. 71, no. 2, pp. 1466-1479, Feb. 2022.
- [59] C. Zhang, S. Wang, and C. Yu *et al.*, "Novel improved particle swarm optimization-extreme learning machine algorithm for state of charge estimation of lithium-ion batteries," *Industrial & Engineering Chemistry Research*, vol. 61, no. 46, pp. 17209-17217, Nov. 2022.
- [60] L. Xia, S. Wang, and C. Yu *et al.*, "Joint estimation of the state-of-energy and state-of-charge of lithium-ion batteries under a wide temperature range based on the fusion modeling and online parameter prediction," *Journal of Energy Storage*, vol. 52, pp. 1-14, Aug. 2022.
- [61] B. Du, Z. Yu, and S. Yi *et al.*, "State-of-charge estimation for second-life lithium-ion batteries based on cell difference model and adaptive fading unscented Kalman filter algorithm," *International Journal of Low-Carbon Technologies*, vol. 16, no. 3, pp. 927-939, Mar. 2021.
- [62] P. Tagade, K.S. Hariharan, and S. Ramachandran *et al.*, "Deep Gaussian process regression for lithium-ion battery health prognosis and degradation mode diagnosis," *Journal of Power Sources*, vol. 445, pp. 1-14, Jan. 2020.